



A novel bioactive tyramine derived Schiff base and its transition metal complexes as selective DNA binding agents

N. Raman^{a,*}, S. Sobha^a, A. Thamarachelvan^b

^a Research Department of Chemistry, VHNSN College, Virudhunagar, Tamil Nadu 626 001, India

^b PG and Research Department of Chemistry, Thiagarajar College, Madurai 625 009, India

ARTICLE INFO

Article history:

Received 21 July 2010

Received in revised form 6 December 2010

Accepted 14 December 2010

Keywords:

Metal complexes

Schiff base

DNA binding

Molecular docking

DNA cleavage

Biological activity

ABSTRACT

A novel tyramine derived Schiff base, 3-4-dimethoxybenzylidene-4-aminoantipyrinyl-4-aminoethylphenol(L) and a series of its transition metal complexes of the type, ML_2Cl_2 where, $M = Cu(II), Ni(II), Co(II)$ and $Zn(II)$ have been designed and synthesized. Their structural features and other properties were deduced from the elemental analysis, magnetic susceptibility and molar conductivity as well as from mass, IR, UV–vis, 1H NMR and EPR spectral studies. The binding properties of these complexes with calf thymus DNA (CT-DNA) were investigated using electronic absorption spectroscopy, viscosity measurement, cyclic voltammetry and molecular docking analysis. The results reveal that the metal(II) complexes interact with DNA through minor groove binding. The interaction has also been investigated by gel electrophoresis. Interestingly, it was found that all the complexes could cleave the circular plasmid pUC19 super coiled (SC) DNA efficiently in the presence of AH_2 (ascorbic acid). The complexes showed enhanced antifungal and antibacterial activities compared to the free ligand.

© 2010 Elsevier B.V. All rights reserved.

1. Introduction

Medical inorganic chemistry has exploited the unique properties of metal ions for the design of new drugs [1]. This has, for instance, demonstrated through numerous biological experiments that DNA is the primary intracellular target for many anticancer drugs, carcinogens and viruses [2–4]. In this regard, chemical modification of nucleic acid by transition metal complexes is of paramount importance for designing chemotherapeutic drugs which regulate gene expression and tools for molecular biology [5]. Transition metal complexes have largely been employed for these purposes not only because of their unique spectral and electrochemical signatures but also due to the fact that the DNA binding and cleaving ability of metal complexes could be tuned by changing the ligand environment. These studies are also important for the development of new probes for nucleic acids and determination of the mechanism of metal ion toxicity [6,7].

Tyramine is widely used as a pharmacological tool to evaluate the role of the sympathetic nervous system on human physiology and pathology [8]. Schiff base of 4-aminoantipyrine and its complexes exhibit a great variety of biological activities such as antitumor, fungicidal, bactericidal, anti-inflammatory and antiviral activities [9–11]. The remarkable biological potencies of these complexes are due to their ability to bind to cellular DNA and cleave

plasmid DNA efficiently [12,13]. However, to the best of our knowledge, no report has yet appeared on the DNA interaction of Schiff base metal complexes of 4-aminoantipyrine derivatives containing the tyramine moiety. Currently, although much attention has been paid to the interaction of DNA with complexes of $Ru(II)$ [14], the other metal ion complexes have attracted much less attention than $Ru(II)$ complexes. This fact prompted us to design a novel DNA binding and cleaving reagent, 3-4-dimethoxybenzylidene-4-aminoantipyrinyl-4-aminoethylphenol (L) and its transition metal(II) complexes.

In this paper, we report the synthesis and characterization of 1:2 type $[ML_2Cl_2]$ complexes where, $M = Cu(II), Ni(II), Co(II)$ or $Zn(II)$ and present their DNA binding and cleaving abilities. A molecular modeling study was performed with special reference to docking to confirm the minor groove binding mode of these complexes to AT base pairs in DNA. Biological activities of the said complexes have also been evaluated. These studies assume significance as they further the comprehension of binding of transition metal complexes to DNA and for developing the next generation of DNA binding and anticancer drugs.

2. Experimental

2.1. Materials and methods

All chemicals used in the present work viz., 4-aminoantipyrine, 3,4-dimethoxy benzaldehyde, tyramine, and metal(II) chlorides were of analytical reagent grade (produced by Merck, Germany).

* Corresponding author. Tel.: +91 9245 165958 (mobile); fax: +91 4562 281338.
E-mail address: drn.raman@yahoo.co.in (N. Raman).

Commercial solvents were distilled and then used for the preparation of ligand and its complexes. CT-DNA and pUC19 DNA were purchased from Bangalore Genei (India). Microanalyses (C, H and N) were performed in Carlo Erba 1108, Heraeus. Molar conductivities in DMSO (10^{-3} M) solution at room temperature were measured using Deep Vision Model-601 digital direct reading deluxe conductivity meter. Magnetic susceptibility measurements of the complexes were carried out by Gouy balance using copper sulphate pentahydrate as calibrant. IR spectra were recorded as KBr pellets on Perkin-Elmer FT-IR 783 Spectrophotometer. NMR spectra were recorded on a Bruker Avance Dry 300 FT NMR Spectrometer in CDCl_3 with TMS as the internal reference. FAB-MS Spectra were recorded with a VGZAB-HS Spectrometer at room temperature in a 3-nitrobenzylalcohol matrix. Electron paramagnetic resonance spectra of the mixed ligand complexes of copper(II) were recorded on a Varian E 112 EPR Spectrometer in DMSO solution both at room temperature (300 K) and at liquid nitrogen temperature (77 K) using TCNE (tetracyanoethylene) as the g-marker. The absorption spectra were recorded using Shimadzu model UV-1601 Spectrophotometer at room temperature.

2.2. Synthesis

2.2.1. Synthesis of 3-4-dimethoxybenzylidene-4-aminoantipyrine

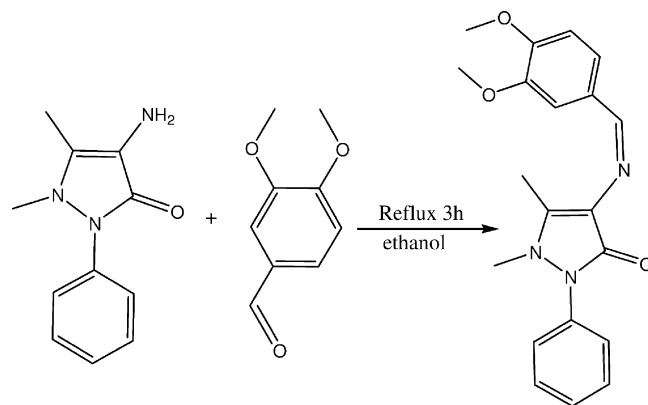
An ethanolic solution of (40 mL) 4-aminoantipyrine (4.06 g, 0.02 mol) was added to an ethanolic solution of 3,4-dimethoxybenzaldehyde (3.14 g, 0.02 mol). The resultant mixture was refluxed for *ca.* 3 h. The solid product formed was filtered and recrystallized from ethanol (Scheme 1).

2.2.2. Synthesis of Schiff base (L)

An ethanolic solution of 3-4-dimethoxybenzylidene-4-aminoantipyrine (3.51 g, 0.01 mol) was added to an ethanolic solution of tyramine (1.37 g, 0.01 mol) and the resultant mixture was refluxed for *ca.* 6 h after the addition of anhydrous potassium carbonate. The potassium carbonate was filtered off from the reaction mixture and the solvent was evaporated. The pale orange solid separated was filtered and recrystallized from ethanol (Scheme 2).

2.2.3. Synthesis of complexes

An ethanolic solution of metal(II) chlorides (1 mmol) was stirred with an ethanol solution of the Schiff base (2 mmol) for *ca.* 2 h on



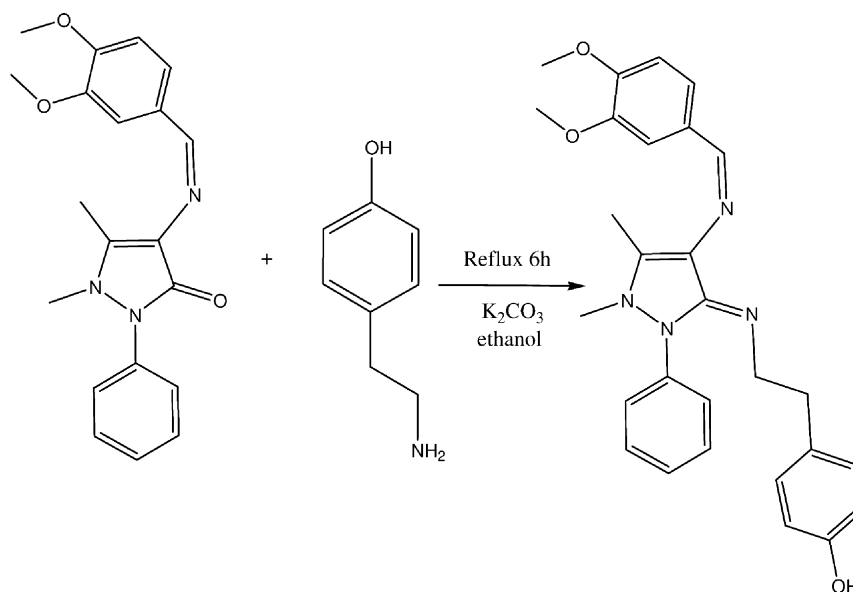
Scheme 1. Synthesis of 3-4-dimethoxybenzylidene-4-aminoantipyrine.

a magnetic stirrer at room temperature. Then the solution was reduced to one-third on a water bath. The solid complex precipitated was filtered off, washed thoroughly with ethanol and dried *in vacuo*.

2.3. DNA binding experiments

2.3.1. Absorption spectroscopic studies

The interactions between metal complexes and DNA were studied using electrochemical and electronic absorption methods. Disodium salt of calf thymus DNA was stored at 4 °C. Solution of DNA in the buffer 50 mM NaCl, 5 mM Tris-HCl (pH 7.2) in water gave a ratio 1.8–1.9, of UV absorbance at 260 and 280 nm, A_{260}/A_{280} , indicating that the DNA was sufficiently free from protein [15]. The concentration of DNA was measured using its extinction coefficient at 260 nm ($6600 \text{ M}^{-1} \text{ cm}^{-1}$). Stock solutions were stored at 4 °C and used no more than 4 days. Doubly distilled water was used to prepare solutions. Concentrated stock solutions of the complexes were prepared by dissolving the complexes in DMSO and diluting suitably with the corresponding buffer to the required concentration for all of the experiments. The data were then fitted to Eq. (1) to obtain the intrinsic binding constant (K_b) values for interaction of the complexes with



Scheme 2. Synthesis of 3-4-dimethoxybenzylidene-4-aminoantipyrinyl-4-aminoethyl-phenol (L).

DNA.

$$\frac{[\text{DNA}]}{\varepsilon_a - \varepsilon_f} = \frac{[\text{DNA}]}{\varepsilon_b - \varepsilon_f} + \frac{1}{[K_b(\varepsilon_b - \varepsilon_f)]} \quad (1)$$

where ε_a , ε_f , and ε_b are the apparent, free and bound metal complex extinction coefficients, respectively. A plot of $[\text{DNA}]/(\varepsilon_b - \varepsilon_f)$ versus $[\text{DNA}]$, gave a slope of $1/(\varepsilon_b - \varepsilon_f)$ and a y-intercept equal to $[K_b/(\varepsilon_b - \varepsilon_f)]^{-1}$, K_b is the ratio of the slope to the y-intercept.

2.3.2. Electrochemical methods

Cyclic voltammetry were performed on a CHI 620C electrochemical analyzer with three electrode system of glassy carbon as the working electrode, a platinum wire as auxiliary electrode and Ag/AgCl as the reference electrode. Solutions were deoxygenated by purging with N_2 prior to measurements.

2.3.3. Viscosity measurements

Viscosity experiments were carried on an Ostwald viscometer, immersed in a thermostated water-bath maintained at a constant temperature at $30.0 \pm 0.1^\circ\text{C}$. CT DNA samples of approximately 0.5 mM, were prepared by sonication in order minimize complexities arising from CT DNA flexibility [16]. Flow time was measured with a digital stopwatch three times for each sample and an average flow time was calculated. Data were presented as $(\eta/\eta_0)^{1/3}$ versus the ratio of metal(II) complexes to DNA, where η is the viscosity of CT DNA solution in the presence of complex, and η_0 is the viscosity of CT DNA solution in the absence of complex. Viscosity values were calculated after correcting the flow time of buffer alone (t_0), $\eta = (t - t_0)/t_0$ [17].

2.4. pUC19 DNA cleavage study

The oxidative cleavage experiment was performed using super coiled pUC19 plasmid DNA Form I ($2 \mu\text{L}$, $10 \mu\text{M}$) in Tris-HCl buffer (50 mM) with 50 mM NaCl (pH 7.2) which was treated with the metal complex ($30 \mu\text{M}$) and ascorbic acid ($10 \mu\text{M}$) followed by dilution with the Tris-HCl buffer to a total volume of $20 \mu\text{L}$. The samples were incubated for 1 h at 37°C . A loading buffer containing 25% bromophenol blue, 0.35% xylene cyanol, 30% glycerol ($3 \mu\text{L}$) was added and electrophoresis performed at 40V for each hour in Tris-acetate-EDTA (TAE) buffer using 1% agarose gel containing $1.0 \mu\text{g}/\text{mL}$ ethidium bromide. The cleavage of DNA was monitored using agarose gel electrophoresis. The gel was visualized by photographing the fluorescence of intercalated ethidium bromide under a UV illuminator. The cleavage efficiency was measured by determining the ability of the complex to convert the super coiled (SC) DNA to nicked circular form (NC) and linear form. Inhibition reaction was also carried out by prior incubation of the pUC19 DNA with DMSO ($4 \mu\text{L}$) (hydroxyl radical scavenger) and sodium azide ($100 \mu\text{M}$) (singlet oxygen scavenger).

2.5. Molecular modeling studies

The interaction of the metal complexes with DNA was also studied by molecular modeling with special reference to docking. All calculations were performed in Open Eye with Fast Rigid Exhaustive Docking using the FRED docking software package. The main function employed for the calculation program was Chemguass 2. Prior to docking, the structure of the metal complexes was constructed and geometry optimized by MM2 force field. The crystal structure of the complex of netropsin with B-DNA dodecamer d(CGCGAATTCGCG)₂ (NDB code GDLB05), was downloaded from Protein Data Bank. During the docking analysis, the binding site of the netropsin drug in the minor groove of the above complex was assigned as the binding site for our metal complexes across

the entire DNA molecule. The docked poses were generated by the exhaustive search and optimization step. FRED selects the single best pose from the set of candidates. This pose is then scored and the score is used to rank ligands in the output hit list. The consensus structure step allows multiple scoring functions to vote for the best docked structure in a rank-by-vote approach.

2.6. Antimicrobial activity studies

The *in vitro* antibacterial and antifungal activities of the ligand and its complexes were tested against the bacteria *Staphylococcus aureus*, *Pseudomonas aeruginosa*, *Escherichia coli*, *Staphylococcus epidermidis* and *Klebsiella pneumoniae* and the fungi *Aspergillus niger*, *Fusarium solani*, *Culvularia lunata*, *Rhizoctonia bataicola* and *Candida albicans*. For the detection of the biocidal activities, the filter paper disc agar diffusion method was used. Pure Streptomycin and Nystatin were used separately as standards for antibacterial and antifungal activity tests respectively. The stock solution was prepared by dissolving the 1 mg of sample in 10 mL of DMSO to give the concentration of $100 \mu\text{g}/\text{mL}$ and the solution was serially diluted in order to find the minimum inhibitory concentration (MIC) value. The suitable medium (nutrient agar for bacteria and potato dextrose agar medium for fungi) was inoculated with the test organisms. The standard solutions of Streptomycin and Nystatin were prepared in DMSO to give concentration of $100 \mu\text{g}/\text{mL}$. The sterilized blank paper discs of 6 mm diameter were impregnated with tested compounds and placed on the surface of the agar plates previously spread with 0.1 mL of overnight culture of microorganisms. The incubation was carried out 24 h for bacteria and 72 h for fungi at 30°C . During the period, the test solution diffused and the growth of the inoculated microorganisms was affected. The inhibition zone was developed, at which the concentration was noted.

3. Results and discussion

The Schiff base ligand, L and its Cu(II), Ni(II), Co(II) and Zn(II) complexes were synthesized and characterized by spectral and elemental analysis data. The complexes were found to be air stable. The ligand was soluble in common organic solvents but their complexes were soluble only in CHCl_3 , DMF and DMSO.

3.1. Elemental analysis and molar conductivity measurements

The results of elemental analysis for the metal complexes were in good agreement with the calculated values (Table 1) showing that the complexes have 1:2 metal-ligand stoichiometry of the type ML_2Cl_2 wherein L acts as a bidentate ligand.

The formation of these complexes may proceed according to the equation given below:



where M = Cu(II), Ni(II), Co(II) and Zn(II).

The metal(II) complexes were dissolved in DMSO and the molar conductivities of 10^{-3}M of their solution at room temperature were measured. The lower conductance values ($18.25\text{--}21.47 \Omega^{-1} \text{cm}^{-2} \text{mol}^{-1}$) of the complexes support their non-electrolytic nature. It also indicates that the chloride anions bind to the metal ions as ligands and do not ionize.

3.2. Mass spectra

The mass spectrum of Schiff base ligand showed peak at m/z 471 corresponding to $[\text{C}_{28}\text{H}_{30}\text{N}_4\text{O}_3]$ ion. Also the spectrum exhibited peaks for the fragments at m/z 200, 150, 122 and 77 corresponding

Table 1
Analytical and physical data of Schiff base ligand and its complexes.

Compound	Yield (%)	Color	Found (calc)%				Formula	$(\Lambda_m)^a$	μ_{eff} (BM)
			M	C	H	N			
[C ₂₈ H ₃₀ N ₄ O ₃]	79	Pale orange	–	71.7 (72.2)	6.4 (6.5)	11.9 (12.3)	471	–	–
[CuC ₅₆ H ₆₀ N ₈ O ₆ Cl ₂]	67	Dark green	5.9 (6.1)	62.5 (62.5)	5.4 (5.6)	10.2 (10.4)	1075	18.25	1.86
[NiC ₅₆ H ₆₀ N ₈ O ₆ Cl ₂]	73	Pale blue	5.2 (5.4)	62.4 (62.8)	5.6 (5.6)	10.2 (10.4)	1071	21.47	3.21
[CoC ₅₆ H ₆₀ N ₈ O ₆ Cl ₂]	61	Pale pink	5.0 (5.0)	62.1 (62.4)	5.2 (5.6)	10.1 (10.4)	1071	19.67	4.88
[ZnC ₅₆ H ₆₀ N ₈ O ₆ Cl ₂]	85	Yellow	5.9 (6.0)	62.3 (62.4)	5.4 (5.6)	10.2 (10.4)	1077	18.76	Diamagnetic

^a The unit of the molar conductance is $\Omega^{-1} \text{ mol}^{-1} \text{ cm}^2$.

to [C₁₁H₁₂N₄]⁺, [C₉H₁₀O₂]⁺, [C₈H₁₀O]⁺ and [C₆H₅]⁺ respectively. The mass fragmentation pattern of the ligand is shown in Scheme 3. The spectra of Cu(II), Co(II), Ni(II) and Zn(II) complexes showed a molecular ion peak [M⁺] at *m/z* 1075, 1071, 1071 and 1077 respectively that are equivalent to their molecular weights. The Cu(II) complex gave a fragment ion peak with loss of 2 chlorine atoms at *m/z* 1005. All these fragments leading to the formation of the species [ML₂]⁺ which further undergoes de-metallation to yield the species [L⁺] giving the fragment ion peak at *m/z* 471.

3.3. IR spectra

The coordination mode and sites of the ligand to the metal ions were investigated by comparing the infrared spectra of the free ligand with its metal complexes. The characteristic phenolic $\nu(\text{OH})$ mode due to the hydroxyl group of tyramine moiety, present in the Schiff base ligand was observed at 3404 cm^{-1} . The appearance of this band in all the complexes indicates that phenolic $\nu(\text{OH})$ group is free from complexation. In the IR spectrum of the Schiff base ligand the band observed at 1614 cm^{-1} was shifted to lower frequency by 21–35 cm^{-1} on complexation, suggesting the coordination of the azomethine nitrogen. In addition, the ligand also revealed a band at 1656 cm^{-1} due to the $\nu(\text{C}=\text{N})$ vibration, originating from the condensation of amino group of tyramine and 3,4-dimethoxybenzalidene-4-aminoantipyrine, was shifted by 23–31 cm^{-1} on complexation. This is further substantiated by the presence of new bands, found in the spectra of the complexes in the regions 503–522 cm^{-1} and 439–445 cm^{-1} which are assigned to $\nu(\text{M}-\text{N})$ (due to tyramine moiety) and $\nu(\text{M}-\text{N})$ (due to 3,4-dimethoxy benzalidene-4-aminoantipyrine moiety) stretching vibrations. Furthermore, the IR spectra of the all complexes showed another band at 345–368 cm^{-1} , which may be due to $\nu(\text{M}-\text{Cl})$ [18] vibrations. Therefore, from the IR spectra, it is concluded that the Schiff base behaves as a bidentate ligand coordinated to the metal ions via the (HC=N), (C=N) and (M-Cl) groups.

3.4. ¹H NMR spectra

The ¹H NMR spectra of the Schiff base and its zinc complex were recorded at room temperature in CDCl₃. ¹H NMR spectrum of the ligand shows a singlet at 5.3 δ which is attributed to the phenolic –OH group of tyramine moiety present in the Schiff base ligand. The presence of this peak noted for the zinc complex confirms the –OH proton free from complexation. The ligand shows the following signals: phenyl multiplet at 6.3–7.4 δ , –CH=N at 9.6 δ , –OCH₃ at 3.9 δ , –C–CH₃ at 3.1 δ , N–CH₃ at 2.5 δ , and –CH₂ at 1.6–2.1 δ . The azomethine proton (–CH=N) signal in the spectrum of the zinc complex is shifted down field compared to the free ligand, suggesting deshielding of azomethine group due to the coordination with metal ion. There is no appreciable change in all other signals of the complex.

3.5. Electronic spectra

The geometry of the metal complexes has been deduced from electronic spectra and magnetic data of the complexes. The electronic spectra of the complexes were recorded in DMSO solution. All the complexes show the high energy absorption band in the region 27,248–33,112 cm^{-1} . This transition may be attributed to the charge transfer band. The electronic spectrum of copper(II) complex displays the d–d transition band in the region 13,606 cm^{-1} [19,20] which is due to ²E_g → ²T_{2g} transition. This d–d band transition band strongly favors a distorted octahedral geometry around the metal ion. The absorption spectrum of nickel(II) complex displays three d–d bands at 14,535, 15,268 and 23,809 cm^{-1} . These bands correspond to ³A_{2g}(F) → ³T_{2g}(F) (ν_1), ³A_{2g}(F) → ³T_{1g}(F) (ν_2) and ³A_{2g}(F) → ³T_{1g}(P) (ν_3) transitions respectively, being characteristic of an octahedral geometry. This geometry is further supported by its magnetic susceptibility value (3.21 BM). The electronic spectrum of cobalt(II) complex displays three d–d transition bands in the region 15,037, 16,529 and 23,752 cm^{-1} which are assigned to ⁴T_{1g}(F) → ⁴T_{2g}(F) (ν_1), ⁴T_{1g}(F) → ⁴A_{2g}(F) (ν_2), and ⁴T_{1g}(F) → ⁴T_{2g}(P) (ν_3) transitions respectively. This indicates that the complex of Co(II) is six coordinate and probably an octahedral geometry, which is also supported by its magnetic susceptibility value (4.88 BM). The complex of Zn(II) is diamagnetic. According to the empirical formula, an octahedral geometry is proposed for this complex.

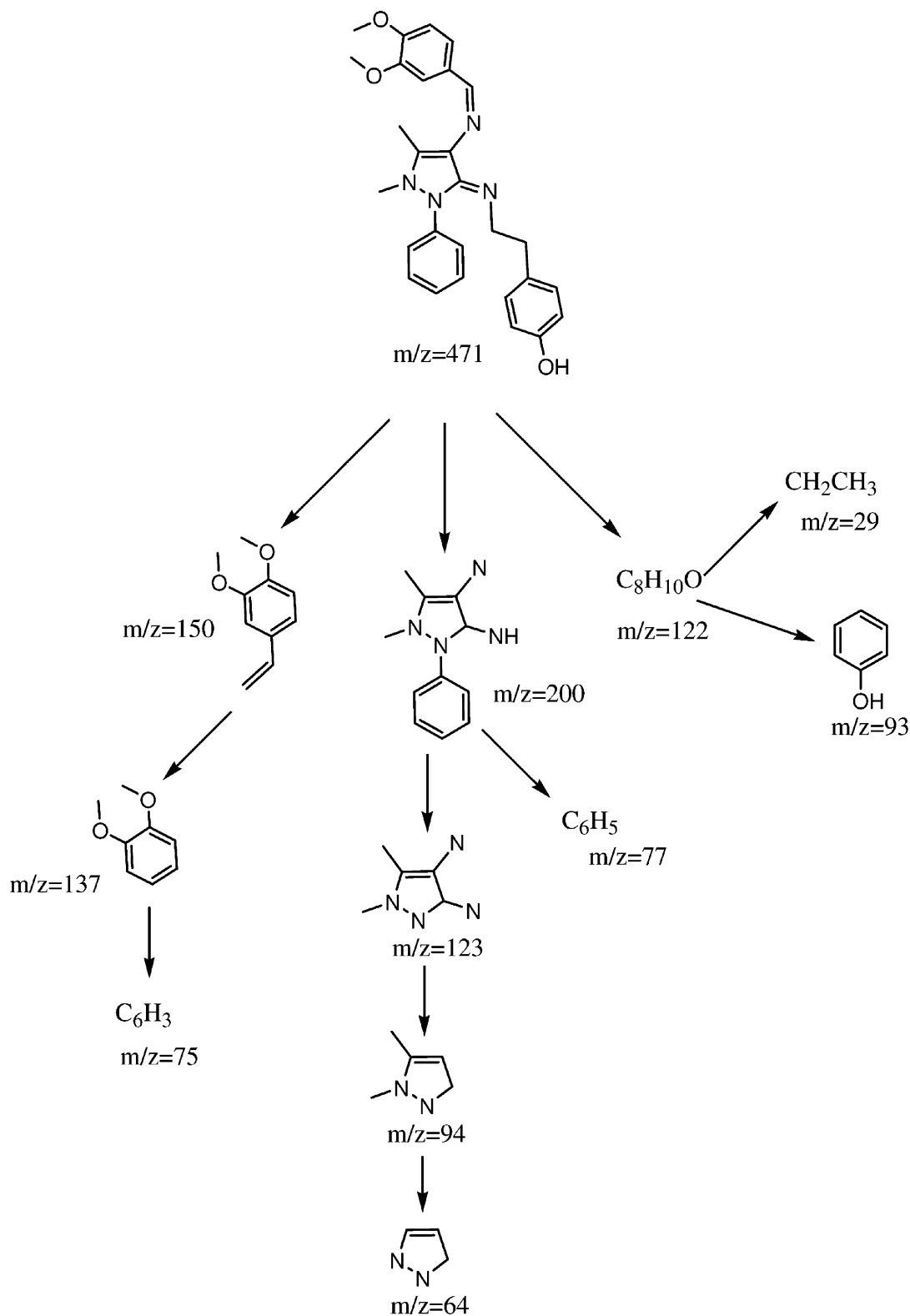
3.6. Electron paramagnetic resonance spectra

The EPR spectrum of copper complex provides information which is important in studying the metal ion environment. The EPR spectra were recorded in DMSO at LNT and at RT. The spectrum of the copper complex at RT shows one intense absorption band in the high field and is isotropic due to the tumbling motion of the molecules. However, this complex at LNT shows well resolved peaks with low field region. The copper complex exhibits the g_{\parallel} value of 2.263 and g_{\perp} value of 2.064. These values indicate that the Cu(II) lies predominantly in the $d_{x^2-y^2}$ orbital, as was evident from the value of the exchange interaction term *G*, estimated from the expression:

$$G = \frac{g_{\parallel} - 2}{g_{\perp} - 2}$$

If $G > 4.0$, the local tetragonal axes are aligned parallel or only slightly misaligned. If $G < 4.0$, significant exchange coupling is present and the misaligned is appreciable. The observed value for the exchange interaction parameter for the copper complex ($G = 4.19$) suggests that the local tetragonal axes are aligned parallel or slightly misaligned and the unpaired electron is present in the $d_{x^2-y^2}$ orbital. This result also indicates that the exchange coupling effects are not operative in the present complex [21].

Based on the above spectral and analytical data, the proposed geometry of the metal(II) complexes is given in Fig. 1.



Scheme 3. Mass fragment pattern of Schiff base.

3.7. DNA binding experiments

3.7.1. Absorption titration

Absorption titration can monitor the interaction of metal complexes and DNA. In general, complex bound to DNA through intercalation usually results in hypochromism and red shift

(bathochromism), due to the strong stacking interaction between aromatic chromophore of the complex and the base pairs of DNA. The absorption spectra of the Cu(II) and Ni(II) complexes in the absence and presence of calf thymus DNA are given in Figs. 2 and 3 respectively. The absorption spectrum of copper complex showed an intensive absorption band at 318.4 nm and

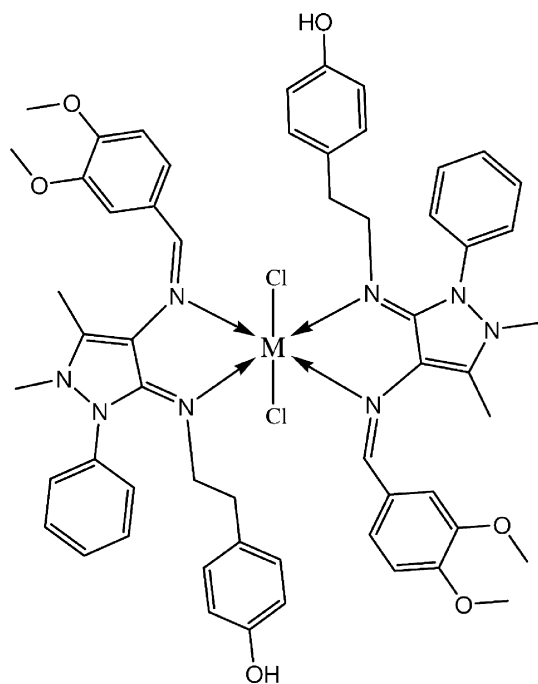


Fig. 1. Proposed structure of the metal complexes $M = \text{Cu(II)}$, Ni(II) , Co(II) and Zn(II) .

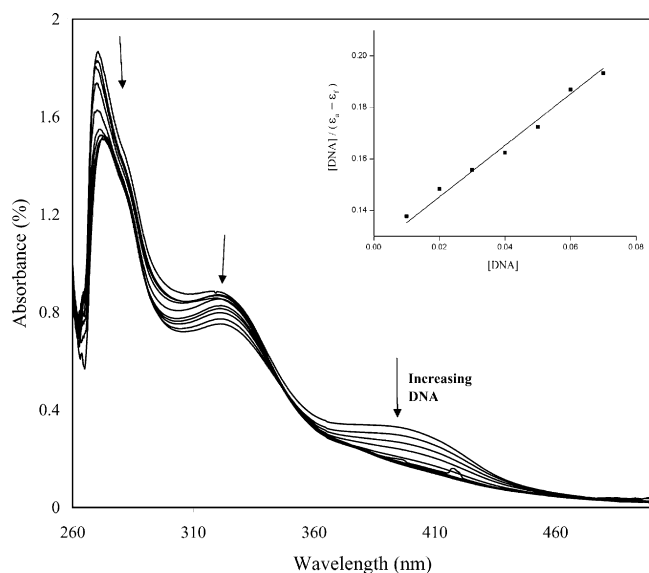


Fig. 2. Absorption spectrum of $[\text{Cu}_{56}\text{H}_{60}\text{N}_8\text{O}_6\text{Cl}_2]$ in buffer $\text{pH} = 7.2$ at 25°C in the presence of increasing amount of DNA. Arrows indicate the changes in absorbance upon increasing the DNA concentration. Inset: plot of $[\text{DNA}]/(\epsilon_a - \epsilon_f)$ versus $[\text{DNA}]$.

Table 2
Electronic absorption spectral properties of Cu(II) , Ni(II) , Co(II) and Zn(II) complexes.

Compound	λ_{max}		$\Delta\lambda/\text{nm}$	$H\%^a$	$K_b^b (\times 10^5 \text{ mol/L})$
	Free	Bound			
$[\text{Cu}_{56}\text{H}_{60}\text{N}_8\text{O}_6\text{Cl}_2]$	397.2	399.2	2.0	25	6.7
	318.8	320.8	2.0	15	
	269.8	272	2.2	18	
$[\text{Ni}_{56}\text{H}_{60}\text{N}_8\text{O}_6\text{Cl}_2]$	320.2	321.4	1.2	24	5.36
	274.2	275.2	1.0	21	
$[\text{Co}_{56}\text{H}_{60}\text{N}_8\text{O}_6\text{Cl}_2]$	305	306.2	1.2	19	1.1
	282.5	284.5	2.0	22	
$[\text{Zn}_{56}\text{H}_{60}\text{N}_8\text{O}_6\text{Cl}_2]$	381.9	384.5	2.6	24	5.5

^a $H\% = [A_{\text{free}} - A_{\text{bound}}]/A_{\text{free}} \times 100\%$.

^b K_b = intrinsic DNA binding constant determined from the UV–vis absorption spectral titration.

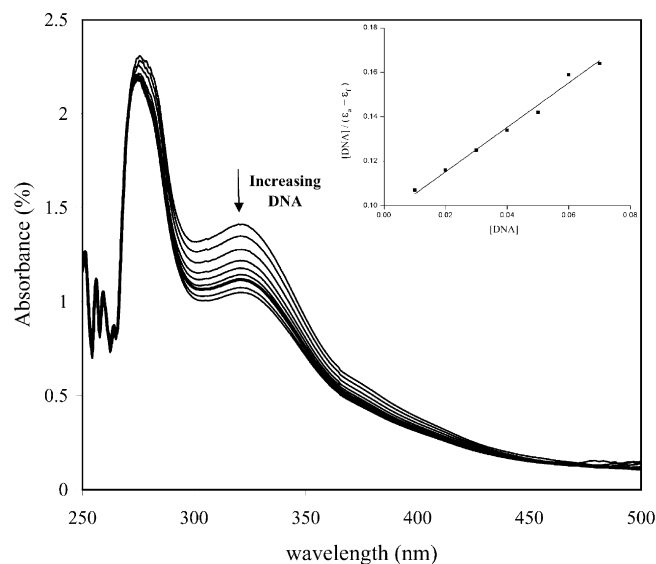


Fig. 3. Absorption spectra of $[\text{Ni}_{56}\text{H}_{60}\text{N}_8\text{O}_6\text{Cl}_2]$ in buffer $\text{pH} = 7.2$ at 25°C in the presence of increasing amount of DNA. Arrows indicate the changes in absorbance upon increasing the DNA concentration. Inset: plot of $[\text{DNA}]/(\epsilon_a - \epsilon_f)$ versus $[\text{DNA}]$.

269.8 nm and a characteristic absorption band at 397.2 nm in 5 mM Tris–HCl, 50 mM NaCl, at pH 7.2 buffer solution respectively. The latter can be attributed to MLCT band, further the intense absorption band with maxima of 305, 282.5 nm for Ni(II) , 320.2, 272 nm for Co(II) and 381 nm for Zn(II) complexes was attributed to π – π^* transition. On increasing the concentration of CT DNA resulted in the minor bathochromic shift in the range ~ 1 –3 nm and significant hypochromicity lying in the range ~ 18 –25% of all the complexes indicating appreciable groove/surface binding propensity of the complexes to the CT DNA. The intrinsic binding constants for Cu(II) , Ni(II) , Co(II) and Zn(II) complexes are found to be 6.7×10^5 , 5.3×10^5 , 1.1×10^5 and $5.5 \times 10^5 \text{ M}^{-1}$ respectively. These values are comparable to the significant DNA groove binding complexes $[\text{Fe}_2(\mu\text{-O})(\text{L-his})_2(\text{phen})_2][\text{ClO}_4]_2$ ($K_b = 1.46 \times 10^5 \text{ M}^{-1}$) and $[\text{Fe}_2(\mu\text{-O})(\text{L-his})_2(\text{dpq})_2][\text{ClO}_4]_2$ ($K_b = 4.55 \times 10^5 \text{ M}^{-1}$), where his = histidine, (phen) = phenanthroline and dpq = dipyrrodoquinoxaline [22]. The small binding constant value also indicates of more surface aggregation and/or groove binding than any interaction to the DNA base pairs. In order to compare the binding strength of the complexes with CT DNA, the intrinsic binding constants (K_b) are obtained by monitoring the changes in the absorbance for the complexes with increasing concentration of DNA. K_b is obtained from the ratio of slope to the intercept from the plot of $[\text{DNA}]/(\epsilon_a - \epsilon_f)$ versus $[\text{DNA}]$. The (K_b) values are shown in Table 2.

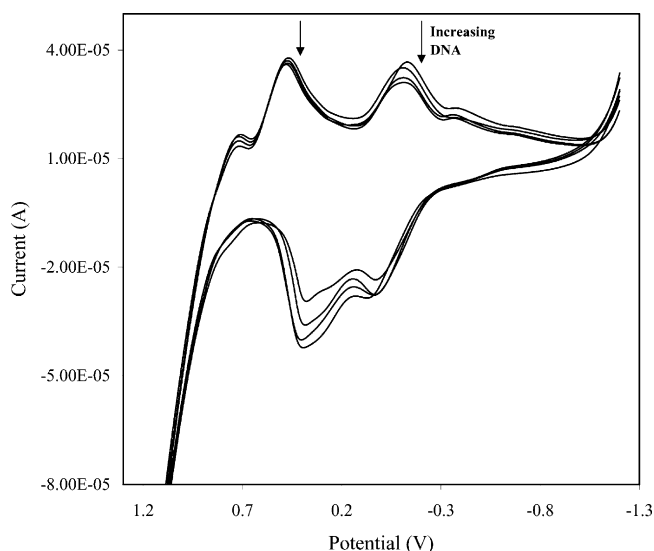


Fig. 4. Cyclic voltammogram of $[\text{CuC}_{56}\text{H}_{60}\text{N}_8\text{O}_6\text{Cl}_2]$ in buffer pH = 7.2 at 25 °C in the presence of increasing amount of DNA. Arrows indicate the changes in voltammetric currents upon increasing the DNA concentration.

3.7.2. Electrochemical studies

The application of cyclic voltammetry to the studies of complexes bound to DNA provides a useful complement to the previously used methods of investigation, such as UV–vis spectroscopy and viscosity measurements. The cyclic voltammograms of $[\text{CuC}_{56}\text{H}_{60}\text{N}_8\text{O}_6\text{Cl}_2]$ and $[\text{NiC}_{56}\text{H}_{60}\text{N}_8\text{O}_6\text{Cl}_2]$ complexes in the absence and in presence of varying amount of DNA are shown in Figs. 4 and 5 respectively. In the absence of CT DNA, the first redox cathodic peak appears at 0.456 V for $\text{Cu(III)} \rightarrow \text{Cu(II)}$ [$E_{\text{p}_a} = 0.422$ V, $E_{\text{p}_c} = 0.456$ V, $\Delta E_{\text{p}} = 0.034$ and $E_{1/2} = 0.44$ V] and in the second redox couple, the cathodic peak appears at -0.122 V for $\text{Cu(II)} \rightarrow \text{Cu(I)}$ [$E_{\text{p}_a} = 0.056$ V, $E_{\text{p}_c} = -0.122$ V, $\Delta E_{\text{p}} = 0.178$ V and $E_{1/2} = -0.033$ V]. The $i_{\text{p}_a}/i_{\text{p}_c}$ ratios of these two redox couples are 0.78 and 1.0 respectively which indicate that the reaction of the complex on the glassy carbon electrode surface is quasi-reversible redox process. The incremental addition of CT DNA to the complexes reveals that the redox couples cause a less negative shift in $E_{1/2}$ and decrease of ΔE_{p} (Table 3). The $i_{\text{p}_a}/i_{\text{p}_c}$ values also decrease in the presence of DNA. Bard has reported [23] $E_{1/2}$, shifted to more positive value the interaction mode was intercalative binding. In contrast, the slight decrease in peak potential and voltammetric currents were occurred and this can be attributed to diffusion of the metal complexes, bound to the large slowly diffusing DNA molecule. In nickel complex, in the absence of CT DNA, the first redox cathodic peak appears at -0.369 V for $\text{Ni(III)} \rightarrow \text{Ni(II)}$ [$E_{\text{p}_a} = 0.745$ V, $E_{\text{p}_c} = -0.369$ V, $\Delta E_{\text{p}} = 1.114$ V and $E_{1/2} = 0.19$ V] and second redox couple cathodic peak appears at -0.0955 V for $\text{Ni(II)} \rightarrow \text{Ni(I)}$

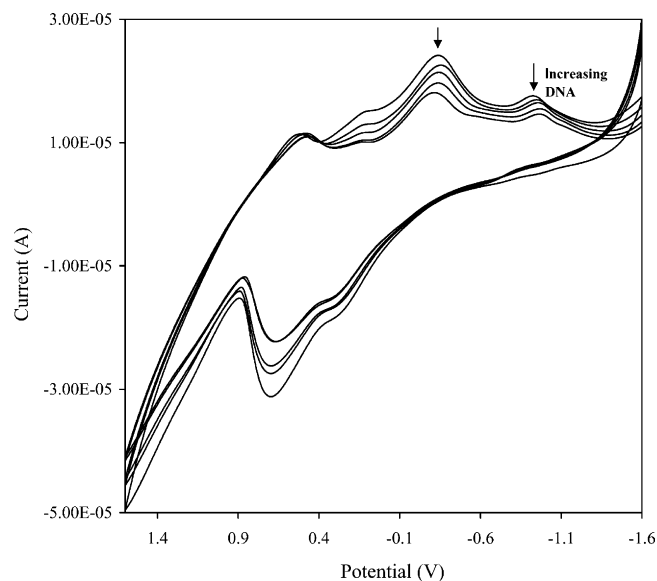


Fig. 5. Cyclic voltammogram of $[\text{NiC}_{56}\text{H}_{60}\text{N}_8\text{O}_6\text{Cl}_2]$ in buffer pH = 7.2 at 25 °C in the presence of increasing amount of DNA. Arrows indicate the changes in voltammetric currents upon increasing the DNA concentration.

[$E_{\text{p}_a} = 0.264$ V, $E_{\text{p}_c} = -0.955$ V, $\Delta E_{\text{p}} = 1.219$ V and $E_{1/2} = 0.345$ V]. In these two redox couples, the ratio of $i_{\text{p}_a}/i_{\text{p}_c}$ is approximately unity which indicates that the reaction of the complex on the glassy carbon electrode surface is quasi-reversible redox process. The incremental addition of CT DNA at the same concentration of the complex causes considerable decrease in the voltammetric currents. In addition, the peak potentials, E_{p_c} and E_{p_a} as well as $E_{1/2}$ had a shift to less negative potential. The drop of the voltammetric currents in the presence of CT DNA can be attributed to diffusion of the metal complexes bound to the large slowly diffusing DNA molecule [24].

For $\text{Co(III)} \rightarrow \text{Co(II)}$ the redox couple cathodic peak appears at -0.152 V in the absence of CT DNA ($E_{\text{p}_a} = 0.602$ V, $E_{\text{p}_c} = -0.152$ V, $\Delta E_{\text{p}} = 0.754$ V and $E_{1/2} = 0.245$ V). The ratio of $i_{\text{p}_a}/i_{\text{p}_c}$ is approximately unity. This indicates the quasi-reversible redox process of the metal complex. The incremental addition of CT DNA to the complexes the redox couples cause a negative shift in $E_{1/2}$ and a decrease in ΔE_{p} . Finally Zn(II) complex exhibits quasi-reversible transfer process with redox couple $[\text{Zn(II)} \rightarrow \text{Zn(0)}]$ cathodic peak appears at -0.536 V in the absence of DNA ($E_{\text{p}_a} = 0.404$ V, $E_{\text{p}_c} = -0.536$ V, $\Delta E_{\text{p}} = 0.940$ V and $E_{1/2} = -0.06$ V). The ratio of $i_{\text{p}_a}/i_{\text{p}_c}$ is 0.74 V. This indicates the quasi-reversible redox process of the metal complex. Incremental addition of DNA on Zn(II) complex shows a slight decrease in the current intensity and negative shift of the oxidation peak potential. The resulting minor changes in the current and potential demonstrate diffusion of the Zn(II) bound to the large

Table 3
Electrochemical parameters for interaction of DNA with Cu(II) , Ni(II) , Co(II) and Zn(II) complexes.

Compound	Redox couple	$E_{1/2}^a$ (V)		ΔE_{p} (V) ^b		$i_{\text{p}_a}/i_{\text{p}_c}$
		Free	Bound	Free	Bound	
$[\text{CuC}_{56}\text{H}_{60}\text{N}_8\text{O}_6\text{Cl}_2]$	$\text{Cu(III)} \rightarrow \text{Cu(II)}$	0.440	0.450	0.034	0.035	0.78
	$\text{Cu(II)} \rightarrow \text{Cu(I)}$	-0.033	-0.066	0.178	0.136	1.80
$[\text{NiC}_{56}\text{H}_{60}\text{N}_8\text{O}_6\text{Cl}_2]$	$\text{Ni(III)} \rightarrow \text{Ni(II)}$	-0.345	-0.373	1.114	1.245	1.30
	$\text{Ni(II)} \rightarrow \text{Ni(I)}$	0.387	0.376	1.219	1.069	1.10
$[\text{CoC}_{56}\text{H}_{60}\text{N}_8\text{O}_6\text{Cl}_2]$	$\text{Co(III)} \rightarrow \text{Co(II)}$	0.245	0.224	0.754	0.833	0.92
$[\text{ZnC}_{56}\text{H}_{60}\text{N}_8\text{O}_6\text{Cl}_2]$	$\text{Zn(II)} \rightarrow \text{Zn(0)}$	-0.066	-0.095	0.940	0.958	0.74

^a Data from cyclic voltammetric measurements; $E_{1/2}$ is calculated as average of anodic (E_{p_a}) and (E_{p_c}) peak potential $E_{1/2} = E_{\text{p}_a} + E_{\text{p}_c}/2$.

^b $\Delta E_{\text{p}} = E_{\text{p}_a} - E_{\text{p}_c}$.

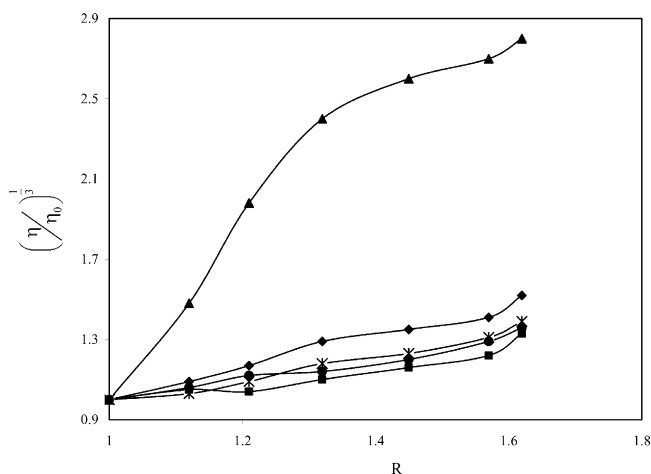


Fig. 6. Effect of increasing amounts of $[\text{CuC}_{56}\text{H}_{60}\text{N}_8\text{O}_6\text{Cl}_2]$ (\blacklozenge), $[\text{NiC}_{56}\text{H}_{60}\text{N}_8\text{O}_6\text{Cl}_2]$ (\circ), $[\text{ZnC}_{56}\text{H}_{60}\text{N}_8\text{O}_6\text{Cl}_2]$ (\bullet), $[\text{CoC}_{56}\text{H}_{60}\text{N}_8\text{O}_6\text{Cl}_2]$ (\blacksquare) and [EB] (\blacktriangle) on the viscosity of DNA. $R = [\text{complex}]/[\text{DNA}]$ or $[\text{EB}]/[\text{DNA}]$.

slowly diffusing DNA molecule. The electrochemical parameters of the Co(II), Ni(II), Cu(II) and Zn(II) complexes are shown in Table 3.

3.7.3. Viscosity measurements

To clarify further the interaction between the metal complexes and DNA, viscosity measurements were carried out. In the absence of crystallographic structure data, hydrodynamic methods which are sensitive to DNA length change are regarded as the least ambiguous and the most critical tests of binding in solution. A classical intercalation model results in lengthening the DNA helix, as base pairs are separated to accommodate the binding ligand, leading to the increase of DNA viscosity. However, a partial and/or non-classical intercalation of ligand may bend (or kink) DNA helix, resulting in the decrease of its effective length and concomitantly its viscosity [25]. The plots of $(\eta/\eta_0)^{1/3}$ versus $[\text{complex}]/[\text{DNA}] = R$, gives a measure of the viscosity changes (Fig. 6). The classical intercalators like ethidium bromide are known to increase the base pair separation resulting an increase in the relative viscosity of the DNA. In contrast, groove (or) surface binding can cause an increase in the effective length of DNA leading to a minor increase in the effective length of DNA solution [26]. All the complexes exhibit minor increase in the relative viscosity of CT DNA suggesting primarily groove binding nature of the complexes.

3.7.4. Molecular docking analysis

The results of spectroscopic titration, viscosity and cyclic voltammetry experiments suggest that Cu(II), Ni(II), Co(II) and Zn(II) complexes do not interact with DNA *via* intercalation. The binding constant values were in the range of 10^5 per mole for all the complexes which indicate the possibility of intercalation of these complexes between the DNA base pairs was little mainly due to less effective stacking forces between the aromatic nucleus and DNA bases. Docking experiments were performed in order to find out the chosen binding site along with preferred orientation of the ligand inside the DNA minor groove. Docking experiments in the energy minimized docked structures suggesting the best possible geometry of the metal complexes located to the AT-rich sequence of the minor groove as shown in Fig. 7.

The structural analysis of docked structures gave significant details about the binding pattern of these complexes. Binding energy of docked metal complexes $[\text{CuC}_{56}\text{H}_{60}\text{N}_8\text{O}_6\text{Cl}_2]$, $[\text{NiC}_{56}\text{H}_{60}\text{N}_8\text{O}_6\text{Cl}_2]$, $[\text{CoC}_{56}\text{H}_{60}\text{N}_8\text{O}_6\text{Cl}_2]$ and $[\text{ZnC}_{56}\text{H}_{60}\text{N}_8\text{O}_6\text{Cl}_2]$ were found to be -120.1 , -110.7 , -105.6 and -119.1 kJ mol^{-1} respectively, correlating well with the experimental DNA binding

values. The more negative the relative binding, the more potent the binding as between DNA and target molecules.

3.7.5. Chemical nuclease activity

The study on the cleavage capacity of transition metal complex to DNA is considerably interesting as it can contribute to understanding the toxicity mechanism of them and to develop novel artificial nuclease. DNA cleavage is controlled by relaxation of super coiled circular form of pUC19 DNA into nicked circular form and linear form. When circular plasmid DNA is conducted by electrophoresis the fastest migration will be observed for the supercoiled form (Form I). If one strand is cleaved, the supercoils will relax to produce a slowed moving open circular form (Form II). If both strands are cleaved a linear form (Form III) will be generated that migrates in between [27,28].

The ability of the complexes in affecting DNA cleavage has been investigated by gel electrophoresis using super coiled pUC19 DNA in 5 mM Tris-HCl/50 mM NaCl buffer solution (pH 7.2). All the complexes are found to exhibit nuclease activity. Fig. 8 shows the result of gel electrophoretic separations of plasmid pUC19 DNA induced by an addition of metal(II) complexes in the presence of AH_2 (ascorbic acid). Under the same conditions, free AH_2 produced no cleavage of pUC19 DNA. All super coiled (Form I) DNA was cleaved to form the mixture of Form II and Form III with the addition of the complex concentration. These phenomena imply that Cu(II), Co(II), Ni(II) and Zn(II) complexes induce intensively the cleavage of plasmid pUC19 DNA in the presence of AH_2 (Fig. 8). In order to clarify the cleavage mechanism of pUC19 DNA introduced by metal(II) complexes, the investigation was carried out further on adding DMSO (hydroxyl radical scavenger). It was found that no inhibition of DNA cleavage was observed indicating that hydroxyl radical is not involved in the cleavage process. On the other hand, addition of sodium azide (singlet oxygen scavenger) did not show any apparent inhibition in the DNA (Fig. 9) which reveals that the singlet oxygen $^1\text{O}_2$ is not responsible for the cleavage reaction (Fig. 10). These observations suggested that all the complexes mediated cleavage reaction did not proceed *via* radical cleavage.

3.8. Antimicrobial screening

3.8.1. Antibacterial activity

The Schiff base complexes have provoked wide interest because they possess a diverse spectrum of biological and pharmaceutical activities. The synthesized ligand and its complexes were tested for their *in vitro* antimicrobial activity. They were tested against the bacteria *S. aureus*, *P. aeruginosa*, *E. coli*, *S. epidermidis*, *K. pneumoniae* by paper disc method. The antibacterial activity of the newly synthesized compounds is presented in Table 4. The results indicate that the ligand exhibits moderate antibacterial activity with respect to the complexes against the same microorganisms under identical experimental conditions. Further, the antibacterial action of Schiff base ligand may be significantly enhanced on the presence of azomethine groups which have chelating properties. These properties may be used in metal transport across the bacterial membranes or to attach to the bacterial cells at a specific site from which it can interfere with their growth. Ligand exhibits MIC in the range of (14.5–16.9 $\mu\text{g/mL}$) against all the pathogens. The copper complex shows better antibacterial activity (MIC, 1.9–2.9 $\mu\text{g/mL}$) against the tested microorganisms than the other complexes which have MIC values in the range 2.7–4.8 $\mu\text{g/mL}$. It may be attributed to the atomic radius and the electronegativity of Cu(II) ions. Current studies reveal that the high atomic radius and electronegative metal ions in their metal complexes exhibit high antimicrobial activity. Higher electronegativity and large atomic radius decreases the effective positive charges on the metal complex molecules which

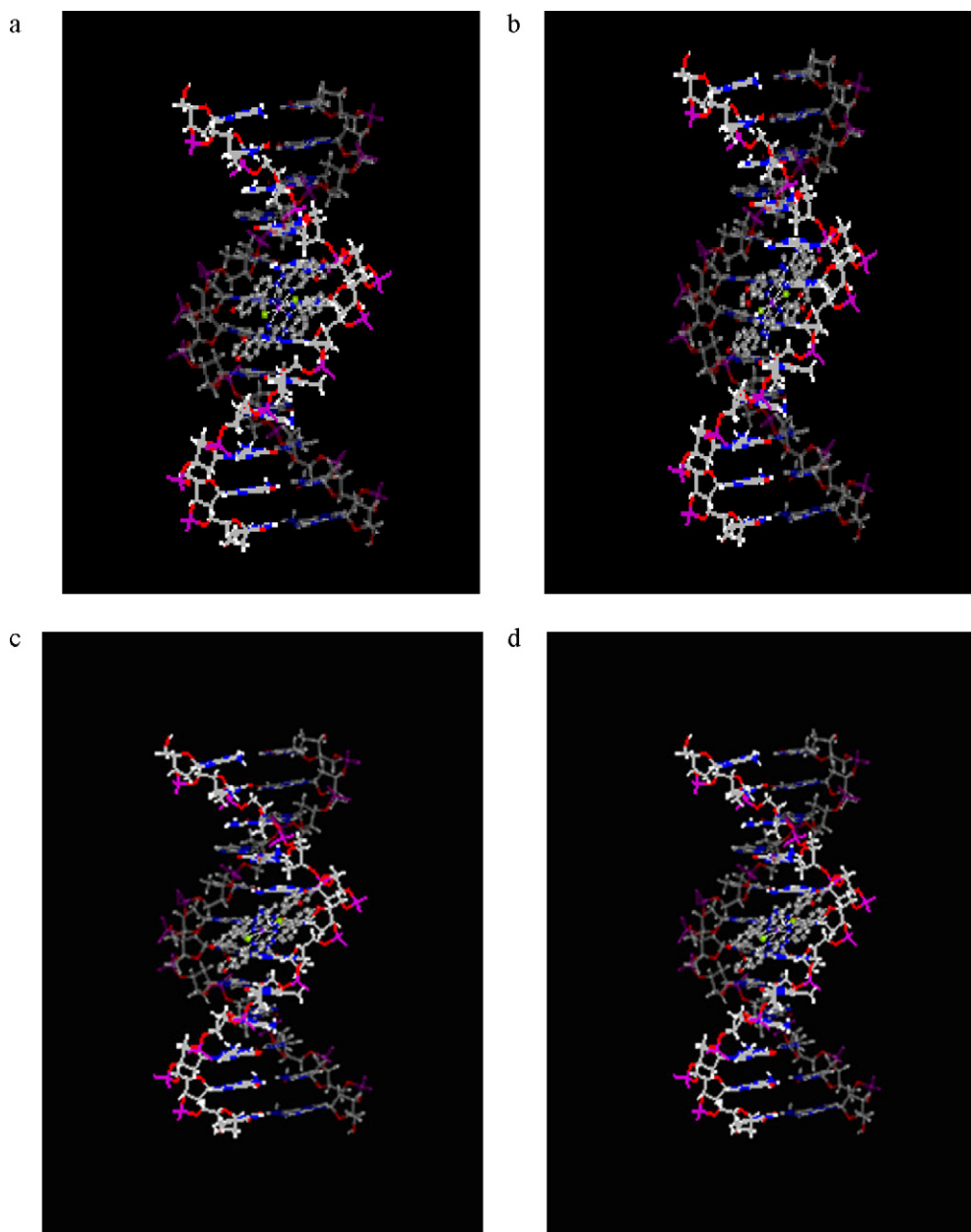


Fig. 7. Interaction of the complexes $[\text{CuC}_{56}\text{H}_{60}\text{N}_8\text{O}_6\text{Cl}_2]$, $[\text{NiC}_{56}\text{H}_{60}\text{N}_8\text{O}_6\text{Cl}_2]$, $[\text{CoC}_{56}\text{H}_{60}\text{N}_8\text{O}_6\text{Cl}_2]$, and $[\text{ZnC}_{56}\text{H}_{60}\text{N}_8\text{O}_6\text{Cl}_2]$ with d(CGCGAATTCGCG) strands of DNA by minor groove binding approach.

facilitates their interaction with the highly sensitive cellular membranes towards the charged particle [29].

3.8.2. Antifungal activity

The Schiff base and its metal complexes were screened for their antifungal activity against *A. niger*, *F. solani*, *C. lunata*, *R. bataicola*

and *C. albicans*. The minimum inhibitory concentration (MIC) values of the investigated compounds are summarized in Table 5. A comparative study of MIC values of ligand (12.9–15.9 $\mu\text{g}/\text{mL}$) and its complexes (2.5–6.8 $\mu\text{g}/\text{mL}$) against all the fungi indicates that the metal complexes exhibit higher antifungal activity than the ligand. Such increased activity on metal chelation can be explained on

Table 4

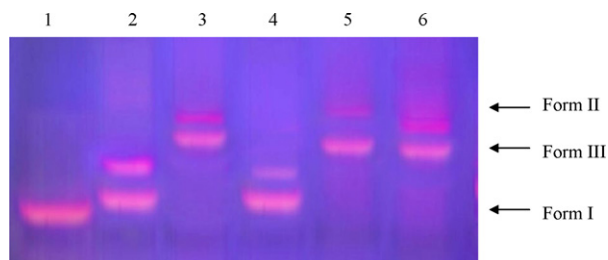
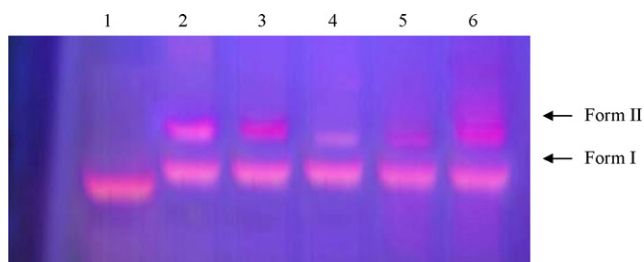
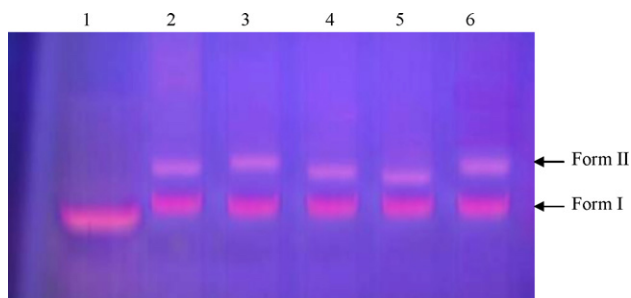
The *in vitro* antibacterial activity of Schiff base and its metal complexes (MIC in $\mu\text{g}/\text{mL}$).

Compound	<i>S. aureus</i>	<i>P. aeruginosa</i>	<i>E. coli</i>	<i>S. epidermis</i>	<i>K. pneumoniae</i>
$[\text{C}_{28}\text{H}_{30}\text{N}_4\text{O}_3]$	16.9	15.8	16.4	16.2	14.5
$[\text{CuC}_{56}\text{H}_{60}\text{N}_8\text{O}_6\text{Cl}_2]$	1.9	2.6	2.2	2.7	2.9
$[\text{NiC}_{56}\text{H}_{60}\text{N}_8\text{O}_6\text{Cl}_2]$	3.1	3.5	3.0	2.7	3.2
$[\text{CoC}_{56}\text{H}_{60}\text{N}_8\text{O}_6\text{Cl}_2]$	3.7	3.4	3.9	4.1	4.2
$[\text{ZnC}_{56}\text{H}_{60}\text{N}_8\text{O}_6\text{Cl}_2]$	3.6	4.8	3.5	3.9	4.4
Streptomycin	1.7	1.9	1.8	1.3	2.3

Streptomycin is used as the standard. MIC ($\mu\text{g}/\text{mL}$) minimum inhibitory concentration, i.e. the lowest concentration to completely inhibit the bacterial growth.

Table 5The *in vitro* antifungal activity of Schiff base and its metal complexes (MIC in $\mu\text{g/mL}$).

Compound	<i>A. niger</i>	<i>F. solani</i>	<i>C. lunata</i>	<i>R. bataicola</i>	<i>C. albicans</i>
[C ₂₈ H ₃₀ N ₄ O ₃]	12.9	13.3	14.5	11.5	15.9
[CuC ₅₆ H ₆₀ N ₈ O ₆ Cl ₂]	2.5	2.3	3.7	4.8	5.9
[NiC ₅₆ H ₆₀ N ₈ O ₆ Cl ₂]	4.2	3.4	4.5	4.7	5.3
[CoC ₅₆ H ₆₀ N ₈ O ₆ Cl ₂]	5.0	5.2	5.9	6.3	6.8
[ZnC ₅₆ H ₆₀ N ₈ O ₆ Cl ₂]	5.3	6.3	6.1	6.5	6.2
Nystatin	1.1	1.6	1.2	1.0	1.5

Nystatin is used as the standard. MIC ($\mu\text{g/mL}$) minimum inhibitory concentration, *i.e.*, the lowest concentration to completely inhibit the fungal growth.**Fig. 8.** Gel electrophoresis diagram showing the cleavage of pUC19 DNA (10 μM) by the Cu(II), Ni(II), Co(II) and Zn(II) complexes in a buffer containing 50 mM Tris-HCl and 50 mM NaCl in the presence of ascorbic acid (AH₂, 10 μM) at 37 °C. Lane 1, DNA control; lane 2, DNA + ligand + AH₂; lane 3, DNA + AH₂ + [CuC₅₆H₆₀N₈O₆Cl₂]; lane 4, DNA + AH₂ + [NiC₅₆H₆₀N₈O₆Cl₂]; lane 5, DNA + AH₂ + [CoC₅₆H₆₀N₈O₆Cl₂]; lane 6, DNA + AH₂ + [ZnC₅₆H₆₀N₈O₆Cl₂].**Fig. 9.** Gel electrophoresis diagram showing the cleavage of pUC19 DNA (10 μM) by the Cu(II), Ni(II), Co(II) and Zn(II) complexes in a buffer containing 50 mM Tris-HCl and 50 mM NaCl in the presence of ascorbic acid (AH₂, 10 μM) and DMSO (4 μL) at 37 °C. Lane 1, DNA control; lane 2, DNA + ligand + AH₂ + DMSO (4 μL); lane 3, DNA + AH₂ + [CuC₅₆H₆₀N₈O₆Cl₂] + DMSO (4 μL); lane 4, DNA + AH₂ + [NiC₅₆H₆₀N₈O₆Cl₂] + DMSO (4 μL); lane 5, DNA + AH₂ + [CoC₅₆H₆₀N₈O₆Cl₂] + DMSO (4 μL); lane 6, DNA + AH₂ + [ZnC₅₆H₆₀N₈O₆Cl₂] + DMSO (4 μL).**Fig. 10.** Gel electrophoresis diagram showing the cleavage of pUC19 DNA (10 μM) by the Cu(II), Ni(II), Co(II) and Zn(II) complexes in a buffer containing 50 mM Tris-HCl and 50 mM NaCl in the presence of ascorbic acid (AH₂, 10 μM) and NaN₃ at 37 °C. Lane 1, DNA; lane 2, DNA + AH₂ + NaN₃; lane 3, DNA + AH₂ + [CuC₅₆H₆₀N₈O₆Cl₂] + NaN₃; lane 4, DNA + AH₂ + [NiC₅₆H₆₀N₈O₆Cl₂] + NaN₃; lane 5, DNA + AH₂ + [CoC₅₆H₆₀N₈O₆Cl₂] + NaN₃; lane 6, DNA + AH₂ + [ZnC₅₆H₆₀N₈O₆Cl₂] + NaN₃.

the basis of Tweedy's chelation theory [30]. Chelation reduces the polarity of the metal ion considerably because of the partial sharing of its positive charge with the donor groups and also due to π -electron delocalization on the whole chelating ring. The lipids

and polysaccharides are some important constituents of the cell wall and membranes which are preferred for metal ion interaction. Apart from this, the cell wall also contains many phosphates, carbonyl and cystenyl ligands which maintain the integrity of the membrane by acting as a diffusion barrier and also provide suitable sites for binding. Furthermore, increased lipophilicity enhances the penetration of the complexes into lipid membrane and blocking of the metal binding sites in the enzymes of microorganisms. These complexes also disturb the respiration process of the cell and thus block the synthesis of the proteins which restricts further growth of the organism.

4. Conclusion

In this paper, the coordination chemistry of a Schiff base ligand obtained from the reaction of 4-aminoantipyrine, 3,4-dimethoxybenzaldehyde and tyramine is described. Cu(II), Ni(II), Co(II), and Zn(II) complexes have been characterized by spectral and analytical data. The IR, electronic transition and g tensor data lead to the conclusion that the Cu(II) ion assumes a distorted octahedral geometry and the other complexes Ni(II), Co(II) and Zn(II) are octahedral in nature. In all the complexes, the ligand acts as bidentate. The DNA-binding properties of synthetic metal complexes have been comprehensively studied by different methods including electronic absorption spectra, viscosity and cyclic voltammetry and docking analysis. The experimental and docking results reveal that all the complexes can interact with DNA through minor groove approach. The complexes are capable of cleaving pUC19 DNA in the presence of AH₂. The antimicrobial screening data reveal that the complexes have higher antimicrobial activity than the free ligand.

Acknowledgements

The authors express their sincere thanks to the College Managing Board, Principal and Head of the Department of Chemistry, VHNSN College, Virudhunagar, India for providing necessary research facilities and financial support. They also wish to acknowledge the help rendered by Thiagarajar College with regard to computational facilities.

References

- [1] P.C.A. Bruijninx, P.J. Sadler, *Curr. Opin. Chem. Biol.* 12 (2008) 197–206.
- [2] V.S. Li, D. Choi, Z. Wang, L.S. Jimenez, M.S. Tang, H. Kohn, *J. Am. Chem. Soc.* 118 (1996) 2326–2331.
- [3] R. Bera, B.K. Sahoo, K.S. Ghosh, S. Dasgupta, *Int. J. Biol. Macromol.* 42 (2008) 14–21.
- [4] S.M. Hecht, *J. Nat. Prod.* 63 (2000) 158–168.
- [5] M.S. Surendra Babu, P.G. Krishna, K.H. Reddy, G.H. Philip, *J. Serb. Chem. Soc.* 75 (2010) 61–74.
- [6] R. Vijayalakshmi, M. Kanthimathi, V. Subramanian, B.U. Nair, *Biochim. Biophys. Acta* 1475 (2000) 157–162.
- [7] K.S. Ksaprak, *Chem. Res. Toxicol.* 4 (1991) 604–615.
- [8] G. Jacob, A. Gamboa, A. Diedrich, C. Shibao, D. Robertson, I. Biaggioni, *J. Hypertens.* 46 (2005) 355–359.
- [9] (a) A.M. Farghaly, A. Hozza, *Pharmazie* 35 (1980) 596–601; (b) T. Hitoshi, N. Tamao, A. Hideyuki, F. Manabu, Takayuki, *Polyhedron* 16 (1997) 3787–3794.

- [10] M.E. Hossain, M.N. Alam, J. Begum, A.M. Akbar, M. Nazimuddin, F.E. Smith, R.C. Hynes, *Inorg. Chim. Acta* 249 (1996) 207–213.
- [11] D. Chiaramonte, J.M. Steiner, J.D. Broussard, K. Baer, S. Gumminger, E.M. Moeller, D.A. Williams, R. Shumway, *Can. J. Vet. Res.* 67 (2003) 182–188.
- [12] N. Raman, R. Jeyamurugan, M. Subbulakshmi, R. Boominathan, C. Yuvarajan, *Chem. Pap.* 64 (2010) 318–328.
- [13] N. Raman, A. Selvan, P. Manisankar, *Spectrochim. Acta Part A* 76 (2010) 161–173.
- [14] G. Sathiyaraj, T. Weyhermuller, B.U. Nair, *Eur. J. Inorg. Chem.* 45 (2010) 284–291.
- [15] J. Marmur, *J. Mol. Biol.* 3 (1961) 208–218.
- [16] J.B. Charies, N. Dattagupta, D.M. Crothers, *Biochemistry* 21 (1982) 3933–3940.
- [17] S. Sathyanarayana, J.C. Daborusak, J.B. Charies, *Biochemistry* 32 (1993) 2573–2584.
- [18] M.J. Kharodawala, M.N. Patel, *Synth. React. Inorg. Met.-Org. Nano-Met. Chem.* 32 (2002) 1483–1495.
- [19] L. Casella, M. Gullotti, *J. Am. Chem. Soc.* 103 (1981) 6338–6347.
- [20] Y. Prashanthi, K. Kiranmai, N.J.P. Subhashini, Shivaraj, *Spectrochim. Acta Part A* 70 (2008) 30–35.
- [21] N. Raman, S. Thalamuthu, J. Dhaveethuraja, M.A. Neelakandan, S. Banerjee, *J. Chil. Chem. Soc.* 53 (2008) 1439–1443.
- [22] M. Roy, T. Bhowmick, R. Santhanagopal, S. Ramakumar, A.R. Chakravarty, *Dalton Trans.* 24 (2009) 4671–4682.
- [23] M.T. Carter, M. Rodriguez, A.J. Bard, *J. Am. Chem. Soc.* 111 (1989) 8901–8911.
- [24] L.-Z. Li, C. Zhao, T. Xu, H.-W. Ji, Y.-H. Yu, G.-Q. Guo, H. Chao, *J. Inorg. Biochem.* 99 (2005) 1076–1082.
- [25] S. Sathyanarayana, J.C. Dabroniak, J.B. Chaires, *Biochemistry* 31 (1992) 9319–9324.
- [26] C. Rajput, R. Rutkaite, L. Swanson, I. Haq, J.A. Thomas, *Chem. Eur. J.* 12 (2006) 4611–4619.
- [27] D.S. Sigman, *Acc. Chem. Res.* 19 (1986) 180–186.
- [28] A.S. Sitlani, E.C. Long, A.M. Pyle, J.K. Barton, *J. Am. Chem. Soc.* 114 (1992) 2303–2312.
- [29] N.A. Negma, M.F. Zakia, M.A.I. Salemb, *Colloids Surf. B: Biointerfaces* 77 (2010) 96–103.
- [30] R. Ramesh, S. Maheswaran, *J. Inorg. Biochem.* 96 (2003) 457–462.